Title

Estimates of Stellar Weak Interaction Rates for Nuclei in the Mass Range A = 65-80

Journal

The Astrophysical Journal Supplement Series, 149(1)

ISSN

0067-0049

Authors

Pruet, Jason

Fuller, George M

Publication Date

2003-11-01

DOI

10.1086/376753

Peer reviewed

The Astrophysical Journal Supplement Series, 149:189–203, 2003 November

ESTIMATES OF STELLAR WEAK INTERACTION RATES FOR NUCLEI IN THE MASS RANGE $A = 65$–80

Jason Pruet
Lawrence Livermore National Laboratory, L-414, P.O. Box 808, Livermore, CA 94551

and

George M. Fuller
Department of Physics, University of California at San Diego, La Jolla, CA 92093-0319
Received 2002 October 30; accepted 2003 May 2

ABSTRACT

We estimate lepton capture and emission rates, as well as neutrino energy loss rates, for nuclei in the mass range $A = 65$–80. These rates are calculated on a temperature/density grid appropriate for a wide range of astrophysical applications including simulations of late time stellar evolution and X-ray bursts. The basic inputs in our single-particle and empirically inspired model are (i) experimentally measured level information, weak transition matrix elements, and lifetimes, (ii) estimates of matrix elements for allowed experimentally unmeasured transitions based on the systematics of experimentally observed allowed transitions, and (iii) estimates of the centroids of the GT resonances motivated by shell model calculations in the *fp* shell as well as by (n, p) and (p, n) experiments. Fermi resonances (isobaric analog states) are also included, and it is shown that Fermi transitions dominate the rates for most interesting proton-rich nuclei for which an experimentally determined ground state lifetime is unavailable. For the purposes of comparing our results with more detailed shell model based calculations we also calculate weak rates for nuclei in the mass range $A = 60$–65 for which Langanke & Martinez-Pinedo have provided rates. The typical deviation in the electron capture and β-decay rates for these $\approx$30 nuclei is less than a factor of 2 or 3 for a wide range of temperature and density appropriate for presupernova stellar evolution. We also discuss some subtleties associated with the partition functions used in calculations of stellar weak rates and show that the proper treatment of the partition functions is essential for estimating high-temperature β-decay rates. In particular, we show that partition functions based on unconverged Lanczos calculations can result in errors in estimates of high-temperature β-decay rates.

Subject heading: nuclear reactions, nucleosynthesis, abundances

On-line material: machine-readable table

1. INTRODUCTION

In this paper we provide estimates for weak interaction rates involving intermediate mass nuclei. Table 1 lists the nuclei we estimate rates for, and Table 2 provides the rates in a similar format and temperature/density grid as the rates provided by Fuller, Fowler, & Newman (1982b). Aufderheide et al. (1990, 1994) have argued that at late times the electron fraction in the Fe core of presupernova stars can be so low that weak processes involving the $A > 65$ nuclei we study are important. Depending on the entropy per baryon, which determines the free proton fraction, electron capture on heavy nuclei may also play an important role during collapse (Bethe et al. 1979; Fuller 1982). In addition, the weak rates we provide for proton-rich nuclei may be used in studies of nucleosynthesis and energy generation in X-ray bursts and other *rp*-process sites (Wallace & Woosley 1981). For the *rp*-process, weak rates are needed for proton-rich nuclei at least up to mass 110. Electron capture and positron decay rates for proton-rich nuclei in the mass range $A = 81$–110, as well as a discussion of some peculiarities of weak rates in the *rp*-process environment, will be presented elsewhere.

The formidable task of calculating the electron and positron capture and emission rates in the conditions characteristic of these astrophysical environments has received more than 4 decades of attention. The first self-consistent calculations to include the effects of the Fermi and Gamow-Teller (GT) resonances as well as the thermal population of these resonances for a broad range of nuclei and thermodynamic conditions were done by Fuller, Fowler, & Newman [1980 (hereafter FFNI), 1982a (hereafter FFNII), 1982b, 1985] and Fuller (1982). FFNI presented a physically intuitive and computationally tractable method for determining the strength and excitation energy of the Fermi and GT resonances. The groundwork for the treatment of these resonances in a thermal environment was laid down by Bethe et al. (1979) and FFNII. The importance of first forbidden transitions, blocking, and thermal unblocking for the very neutron-rich nuclei present during collapse was pointed out by Fuller (1982). Cooperstein & Wambach (1984) calculated electron capture rates for these nuclei by estimating the parity forbidden matrix elements as well as the effects of thermal unblocking of the allowed GT^+ strength.

The last 2 decades have seen a great increase in our understanding of weak interaction systematics in intermediate mass nuclei. There are now semidirect measurements of the GT strength distribution for roughly 40 nuclei from forward angle (n, p) and (p, n) scattering experiments. There are also shell model calculations for the strength distribution for some 400 nuclei in the *fp* shell (Caurier et al. 1999; Langanke & Martinez-Pinedo 2000), as well as a number of RPA and QRPA calculations of the GT resonance in heavier nuclei. One consequence of these studies, first hinted at in the early Lanczos calculations of Bloom & Fuller (1985), is that the FFN prescription misses some important systematics

TABLE 1
RANGE OF Z FOR FIXED A

A	Z Range[a]
66	25–34
67	25–34
68	26–34
69	25–36
70	27–36
71	27–36
72	27–36
73	28–37
74	28–37
75	28–38
76	28–38
77	29–39
78	29–40
79	29–40
80	30–40

[a] For the most neutron (proton) rich element(s) of a given A, we do not calculate a rate in the β^+ (β^-) direction.

in assigning the centroid of the GT resonance. The influence of this misassignment on the rates was discussed by Aufderheide et al. (1996), Caurier et al. (1999), and Langanke & Martinez-Pinedo (2000, hereafter LMP). Langanke & Martinez-Pinedo (2000) also provided updated calculations of the rates for $A \leq 65$ based on large-scale shell model calculations.

We attempt to remedy the misassignment of the GT centroids. Other than this and a different treatment of high-temperature partition functions, our strategy for calculating weak rates for $A \geq 65$ is essentially the FFN approach. In this approach the rates are broken into two pieces: a low part consisting of discrete transitions between individual levels and a high part involving the Fermi and GT resonances. This approach is valid provided that discrete transitions between high-lying levels never dominate the rates. In addition, available experimental information for logft-values and level energies, parities, and spins is used. The inclusion of this much data for more than 100 nuclei is a difficult task, and would not be possible without the Web-based nuclear structure databases (in particular, those provided by nudat and the table of isotopes).

The simple FFN approach for estimating weak rates may be the most natural framework for incorporating experimentally determined nuclear properties. Additionally, a virtue of using this semiempirical schematic approach is that we can easily see where the key nuclear uncertainties are. Our work can then serve as a catalyst for more detailed follow-up nuclear structure studies for important rates.

In the next section we present a discussion of the formalism for calculating weak rates. In § 3 we discuss the assignment of experimentally unknown matrix elements for allowed, discrete state transitions. This discussion is based on the systematics of experimentally observed weak transitions. In § 4 we present a simple approach for estimating the position of the GT resonances and make some comparison with data and shell model calculations. The calculation of rates in a high-temperature environment is treated in § 5. We also discuss in § 5 some subtleties associated with the proper partition function to be used in these calculations. Section 6 gives some comparisons of our estimates for the rates with those provided by Langanke & Martinez-Pinedo. Finally, we conclude with a discussion of the results.

2. WEAK RATES FORMALISM

The total decay rate for a nucleus in thermal equilibrium at temperature T is given by a sum over initial parent states i and final parent states j;

$$\lambda = \sum_i P_i \sum_j \lambda_{ij} \ , \tag{1}$$

where the population factor for a parent state i with excitation energy E_i and angular momentum J_i is

$$P_i = \frac{(2J_i + 1)e^{-E_i/kT}}{Z} \ , \tag{2}$$

TABLE 2
WEAK INTERACTION RATES FOR NUCLEI IN THE MASS RANGE $A = 65$–80

			$Z = 26, N = 40 \rightarrow Z = 25, N = 41$			$Z = 25, N = 41 \rightarrow Z = 26, N = 40$		
$T/10^9$ K	log(ρY_e[g cm^{-3}])	U_F[a]	log(λ_{em})[b]	log(λ_{cap})[c]	log($\dot{e}_\nu$)[d]	log(λ_{em})[b]	log(λ_{cap})[c]	log($\dot{e}_\nu$)[d]
0.01	1.0	−0.003	−100.000	−100.000	−100.000	1.021	−100.000	1.878
0.10	1.0	−0.058	−100.000	−100.000	−100.000	1.021	−54.584	1.878
0.20	1.0	−0.134	−100.000	−100.000	−100.000	1.021	−27.509	1.878
0.30	1.0	−0.218	−100.000	−100.000	−100.000	1.022	−18.193	1.878
0.40	1.0	−0.307	−100.000	−100.000	−100.000	1.022	−13.393	1.878
0.50	1.0	−0.399	−100.000	−100.000	−100.000	1.023	−10.431	1.879
0.60	1.0	−0.478	−100.000	−100.000	−100.000	1.024	−8.534	1.880
0.70	1.0	−0.503	−100.000	−100.000	−100.000	1.024	−7.542	1.881
0.80	1.0	−0.509	−100.000	−100.000	−100.000	1.025	−6.908	1.882
0.90	1.0	−0.510	−100.000	−84.103	−84.732	1.026	−6.423	1.882
1.00	1.0	−0.511	−100.000	−75.945	−76.528	1.026	−6.030	1.883

NOTE.—Table 2 is available in its entirety in the electronic edition of the *Astrophysical Journal Supplement*. A portion is shown here for guidance regarding its form and content.

[a] Electron Fermi energy in MeV.

[b] Rate for charged lepton (e^+ or e^-) emission in units of (nucleus s^{-1})$^{-1}$.

[c] Rate for charged lepton capture in units of (nucleus s^{-1})$^{-1}$.

[d] Total (i.e., for charged lepton capture and emission) neutrino energy loss rate in units of MeV (nucleus s^{-1})$^{-1}$.

with

$$Z = \sum_i (2J_i + 1) e^{-E_i/kT} \tag{3}$$

the nuclear partition function. Here λ_{ij} is the specific weak transition rate between initial parent state i and daughter state j and is formally given by

$$\lambda_{ij} = \frac{\ln 2}{(ft)_{ij}} f_{ij} \ , \tag{4}$$

where

$$\frac{1}{(ft)_{ij}} = \frac{1}{(ft)^{\rm F}_{ij}} + \frac{1}{(ft)^{\rm GT}_{ij}} \tag{5}$$

and where the relation between ft-values and the appropriate Gamow-Teller or Fermi matrix element is

$$(ft)^{\rm GT}_{ij} \approx \frac{10^{3.59}}{|M_{\rm GT}|^2_{ij}} \ , \tag{6}$$

$$(ft)^{\rm F}_{ij} \approx \frac{10^{3.79}}{|M_{\rm F}|^2_{ij}} \ . \tag{7}$$

Here the total Gamow-Teller matrix element between initial parent state $|\psi^P_i\rangle$ and final daughter state $|\psi^D_f\rangle$ is

$$|M_{\rm GT}|^2_{ij} = |\langle \psi^D_f | \sum_n \sigma_n (\tau_\pm)_n |\psi^P_i\rangle|^2 \ , \tag{8}$$

where the sum is over all nucleons. The GT strength satisfies the sum rule

$$\begin{aligned} S_{\beta^-} - S_{\beta^+} &\equiv \sum_f |\langle \psi^D_f | \sum_n \sigma_n (\tau_-)_n |\psi^P_i\rangle|^2 \\ &\quad - |\langle \psi^D_f | \sum_n \sigma_n (\tau_+)_n |\psi^P_i\rangle|^2 \\ &= 3(N - Z) \ . \end{aligned} \tag{9}$$

Similarly, the Fermi matrix element is

$$\begin{aligned} |M_{\rm F}|^2 &= |\langle \psi^D_f | \sum_n (\tau_\pm)_n |\psi^P_i\rangle|^2 \\ &= T(T+1) - T_z(T_z - 1) = |N - Z| \ . \end{aligned} \tag{10}$$

This equation is derived by noting that $[T_+, T_-] = 2T_z = (N - Z)$.

The phase space factors for $\beta^\pm$-decay are

$$f_{ij} = \int_1^{q_n} w^2 (q_n - w)^2 G(\pm Z, w)(1 - f_\mp)(1 - f_\nu) dw \tag{11}$$

and for electron/positron capture are

$$f_{ij} = \int_{w_l}^{\infty} w^2 (q_n + w)^2 G(\pm Z, w) f_\mp (1 - f_\nu) dw \ , \tag{12}$$

where the upper (lower) signs are for electrons (positrons), $q_n = (M_p - M_d + E_i - E_j)/m_e c^2$, and where M_p is the nuclear mass of the parent and M_d is the nuclear mass of the daughter. The threshold is $w_l = 1$ for $q_n > -1$ and $w_l = |q_n|$ for $q_n < -1$. The lepton occupation factors are

$$f_\pm = \left[\exp \frac{U - U^\pm_{\rm F}}{kT} + 1 \right]^{-1} \tag{13}$$

where the minus sign is for electrons, the plus sign is for positrons, U is the electron kinetic energy and $U^\mp_{\rm F}$ the kinetic chemical potential (total chemical potential is here defined to include the electron rest mass). The factor $G(\pm Z, w)$ is the coulomb wave correction factor defined in terms of the Fermi factor F

$$G(\pm Z, w) \equiv \frac{p}{w} F(\pm Z, w) \tag{14}$$

as discussed in FFNI.

Neutrino energy loss rates are calculated in the same way as the decay rates, but with the phase space factor f_{ij} replaced by

$$f^\nu_{ij} = \int_1^{q_n} w^2 (q_n - w)^3 G(\pm Z, w)(1 - f_\mp)(1 - f_\nu) dw \tag{15}$$

for charged lepton emission, and by

$$f^\nu_{ij} = \int_{w_l}^{\infty} w^2 (q_n + w)^3 G(\pm Z, w) f_\mp (1 - f_\nu) dw \tag{16}$$

for charged lepton capture. The sign convention here is the same as that for f_{ij} above, and the energy loss calculated in this way is in units of $m_e c^2\ {\rm s}^{-1}$.

3. ASSIGNMENT OF UNMEASURED, ALLOWED TRANSITION MATRIX ELEMENTS

As in FFN, we break the rates λ_{ij} into two distinct components: discrete transitions between low-lying levels and transitions involving states in the Fermi or GT resonance carrying total weak strength ($|M_{\rm GT}|^2 + |M_{\rm F}|^2$) of order 1 or greater. Discrete state transitions between low-lying states in the parent and daughter are important when the capturing lepton energies are too low to reach resonance states in the daughter or when the temperature is too low to thermally populate parent levels with fast transitions to daughter states. To estimate matrix elements between low-lying parent and daughter levels, FFN adopted the simple prescription that all transitions not forbidden by the selection rules have some average matrix element characteristic of a group of nuclei. We adopt a similar procedure, but here we assign a "characteristic $\log ft$" value, which depends on nuclear mass range, to allowed and experimentally unmeasured transitions. The validity of this approach can be addressed by looking at the systematics of matrix elements for experimentally observed β^+/ec and β^--decays.

Figures 1, 2, and 3 show the characteristic $\log ft$-value for all nuclei in the mass range $A = 65$–80 for which there is experimentally determined weak decay information. By "characteristic $\log ft$" we mean here the $\log ft$-value obtained by assuming that all of the measured discrete strength is spread uniformly over all states in the daughter for which the selection rules do not forbid a transition and for which the Q-value is positive (i.e., the decay is energetically allowed). This estimated number of allowed transitions ($n_{\rm allow}$) for each nucleus is shown on the x-axis. The determination of $n_{\rm allow}$ is difficult because of uncertainties in the angular momentum and spin assignments of levels. Where the angular momentum of a given level is uncertain we have adopted the middle value if more than two possibilities are listed, and the largest value if only two possibilities are given. Where the parity is listed, but uncertain, we have

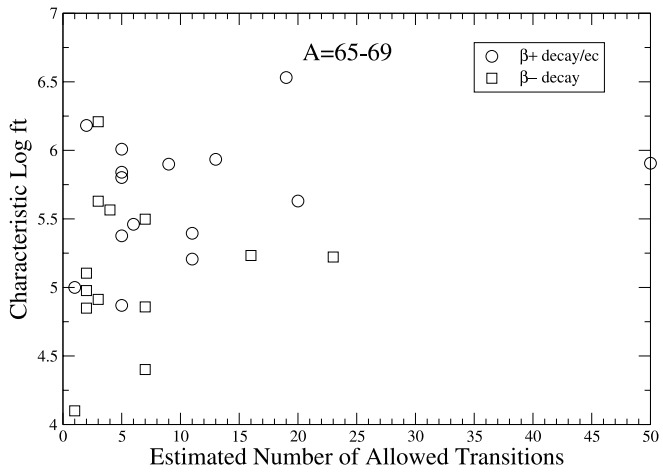

FIG. 1.—Systematics of experimentally determined log ft-values for nuclei with $65 \leq A < 70$.

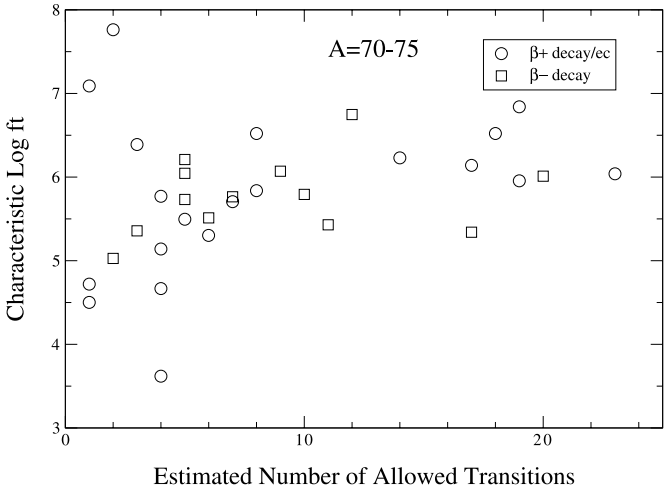

FIG. 2.—Systematics of experimentally determined log ft-values for nuclei with $70 \leq A \leq 75$.

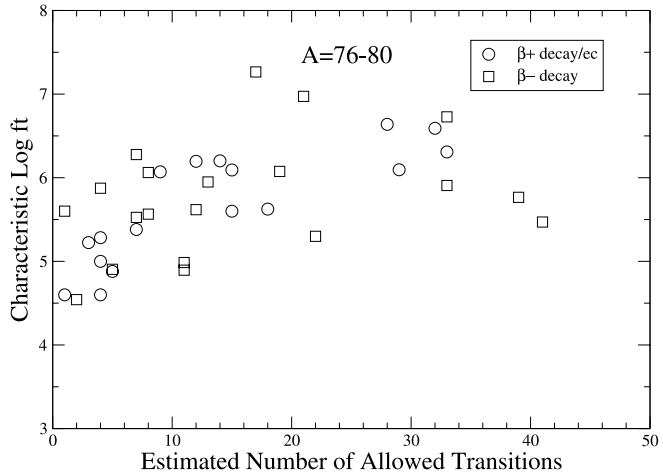

FIG. 3.—Systematics of experimentally determined log ft-values for nuclei with $75 < A \leq 80$.

adopted the tentative value. Transitions involving a level for which no spin or parity information is given are labeled as forbidden. For consistency, these are the same conventions followed in the determination of whether an experimentally unmeasured transition is allowed and assigned a characteristic log ft-value in our calculation of weak rates.

For illustration, consider the β-decay of ^{66}Co. Experimentally it is observed that ^{66}Co decays in this channel to two states in ^{66}Ni, one with a log ft of 4.21 and the other with $\log ft = 4.75$. By examining the experimentally studied levels in ^{66}Ni it is seen that there are seven levels that have spins and parities consistent with allowed decay from ^{66}Co. The characteristic log ft for ^{66}Co is then defined as $-\log_{10}[(1/7)(10^{-4.21} + 10^{-4.7})] = 4.93$. Our definition of the characteristic log ft is rough in that it neglects the experimental difficulties associated with measuring weak transitions. In particular, uncertainties arising from the possibility of the feeding of daughter states from higher lying states have not been accounted for, nor has the difficulty of observing near-threshold transitions. Nonetheless, a case may be made from these figures that the assumption of an average matrix element is a reasonable one, particularly when several transitions are involved. For example, for nuclei with $65 \leq A < 70$, only one nucleus with $n_{\text{allow}} > 2$ has a characteristic log ft differing from 5.4 by more than 1, and for nuclei in the range $70 \leq A \leq 80$ only five nuclei with $n_{\text{allow}} > 2$ have a characteristic log ft differing from 5.7 by more than 1. It should be noted that estimates based on characteristic log ft-values are generally less accurate than estimates based on detailed shell model calculations. For example, for nuclei with well-studied level structures, estimates of ground state lifetimes based on a characteristic log ft are typically in error by a factor of 3 or 4. Note, though, that we use experimentally determined half-lives or strength distributions in place of characteristic log ft-values whenever an experimental lifetime is available.

In this work we take a characteristic log ft of 5.4 for nuclei with $A < 70$, and a characteristic log ft of 5.7 for nuclei with $A \geq 70$. An alternative approach for estimating these matrix elements would be to assign log ft-values from a statistical distribution. Our procedure should give a reasonable estimate of the rates when several transitions contribute nearly equally to the rate. However, our estimated rate is obviously subject to uncertainty when only one or two experimentally unknown transitions dominate.

An important class of nuclei for which a treatment of the decay of low-lying excited states in terms of a characteristic log ft is inappropriate are the proton-rich even-even nuclei with nearly closed neutron and proton subshells. These can have anomalously large $0^+ \rightarrow 1^+$ GT transitions, with $\log ft \lesssim 4$ in many cases. In X-ray burst environments, with temperatures $kT \sim 0.25$ MeV, the first 2^+ excited state in these nuclei can be appreciably thermally populated. The thermal β^+-decay rate of the nucleus depends sensitively on whether this 2^+ state also decays with anomalously large matrix elements. Schatz et al. (1998) studied this question for ^{68}Se and ^{72}Kr, whose ground state decays are characterized by fast $0^+ \rightarrow 1^+$ transitions, and found that the 2^+ state decays more rapidly than the ground state. We incorporate this trend in our calculations for the four nuclei (^{72}Kr, ^{74}Kr, ^{76}Sr, ^{78}Sr) with fast $0^+ \rightarrow 1^+$ transitions. For these nuclei we assume that the first 2^+ state has a strength distribution identical in shape, but with matrix elements twice as large, as the strength distribution from the 0^+ ground state. For

^{68}Se and ^{72}Kr this gives low-temperature decay rates within $\sim$30% of those calculated by Schatz et al.

It should be emphasized that some of the near proton drip line nuclei, for which experimentally determined level and weak decay information are incomplete, are not properly addressed by our largely experimentally based approach. An understanding of the thermal weak decay of these nuclei will likely depend on the resolution of many unresolved questions about their structure. Consequently, our estimates of the weak decay for these nuclei are simple—experimental lifetimes where they are available, and trends suggested by the study of Schatz et al. for the decay of a few important 2^+ states. Another nucleus that is known to be important in determining the nuclear flow in X-ray bursts is ^{80}Zr. Though the excitation energy of the first 2^+ excited state for this nucleus is experimentally known, the level structure in the β^+ daughter is so poorly known that an estimate of the 2^+ decay rate based on characteristic logft-values is not possible. For this nucleus we have made the assumption that the first 2^+ state decays at the same rate as the ground state. This is likely not correct. Our calculation for this nucleus of the decay at low temperatures of states in the "back resonance" (§ 5) is also uncertain. It seems that a shell model calculation capable of reliably estimating the 2^+ (and 4^+) lifetime is needed for a better estimate. The situation for proton-rich nuclei is not as grim as it might first appear since, as we show below, many of the near proton-drip nuclei have thermal decays that are dominated by the reliably estimated Fermi transition.

4. THE FERMI AND GAMOW-TELLER RESONANCES

In this section the Fermi and Gamow-Teller resonances are discussed. Ideally, our description of the GT resonance would be so well resolved that the inclusion of experimentally determined lifetimes, level parameters, and logft systematics would be unnecessary. However, without more detailed structure calculations, the best we can hope for is a reliable estimate of the gross properties of the GT resonance. The careful use of experimental measurements, outlined above, is an attempt to get at the fine details needed for a description of transitions between low-lying levels. Because the characteristic logft was designed to account for the β^+/β^--decay of low-lying states, we do not include GT resonance strength within the Q-window for the decay of a state (the exception to this is the decay of "back resonances" discussed below). In the cases where the prescription discussed below places strength within the Q-window for a decay, we push that strength in our calculations up to $Q = 0$.

The Fermi resonance $|F_i\rangle$ corresponding to a given state $|\psi_i\rangle$ is generated by application of the isospin raising or lowering operator, $|F_i\rangle = T_\pm|\psi_i\rangle$ (eq. [10]). The selection rules for Fermi transitions are $\Delta\pi = \Delta T = \Delta J = 0$. Because $\Delta T = 0$ and because (with the exception of odd-odd $N = Z$ nuclei) the ground state of a nucleus generally has the lowest possible isospin, there typically is only nonzero Fermi strength for transitions from a nucleus with greater isospin $T^>$ to a nucleus with lesser or equal isospin $T^<$. Since the nuclear part of the Hamiltonian ($H_{\rm nuc}$) is isospin independent and the electromagnetic part is small in comparison, the resonance generated by $T_\pm$ is narrowly concentrated about the IAS. The excitation energy can be estimated from the difference in Coulomb binding energy of the parent and daughter nucleus. FFNI gives a useful approximation for the excitation energy of the IAS in the daughter nucleus:

$$E_{\rm IAS} = \Delta_p - \Delta_d \mp 0.7824 \pm 1.728 \min(Z_p, Z_d)/R \ , \quad (17)$$

where $R \approx 1.12A^{1/3} + 0.78$ is the nuclear radius in fm, p and d refer to the parent and daughter, respectively, Δ is the atomic mass excess in MeV, and $E_{\rm IAS}$ is in MeV. The upper signs in the above equation correspond to $(Z, N) \rightarrow (Z + 1, N - 1)$ transitions for neutron-rich parents, while the lower signs correspond to $(Z, N) \rightarrow (Z - 1, N + 1)$ transitions for proton-rich parents. Equation (17) agrees well with measured and shell model predictions for IAS energies.

The Gamow-Teller operator is

$$\mathrm{GT}_\pm = \sum_n \sigma\tau^\pm(n) \ , \quad (18)$$

where the sum is over all nucleons n. The collective GT resonance state $|\mathrm{CGT_i}\rangle$ corresponding to a given parent state $|\psi_i\rangle$ is given by application of the GT operator, $|\mathrm{CGT_i}\rangle = \mathrm{GT}|\psi_i\rangle$. The selection rules for GT transitions are $\Delta\pi = 0$, $\Delta J = 0, \pm 1$ no $0 \rightarrow 0$, and $\Delta T = 0, \pm 1$. The GT strength distribution is harder to characterize because $H_{\rm nuc}$ is strongly spin dependent. Since $[H_{\rm nuc}, \mathrm{GT}_\pm] \neq 0$, the GT strength can be fragmented over many daughter states. However, in practice the stellar weak rates are usually determined by the total strength and the centroid of the strength in excitation energy (provided that low-lying discrete transitions are well accounted for).

The strength in the GT resonance was also estimated by FFN in a zeroth-order shell model picture. In this picture the lowest shell orbitals are filled with nucleons, and the total strength is taken to be the sum of the contributions from each pair of single-particle orbitals:

$$|M_{\rm GT}|^2 = \sum_{if} \frac{n_p^i n_h^f}{2j_f + 1} |M_{\rm GT}^{sp}|_{if}^2 \ . \quad (19)$$

Here "i" and "f" denote initial and final orbitals ($|\phi_i\rangle$ and $|\phi_f\rangle$), respectively, n_p and n_h denote the number of particles and holes in these orbitals, and $M_{\rm GT}^{sp} = \langle\phi_f|\mathrm{GT}|\phi_i\rangle$ is the single-particle matrix element connecting the initial and final states. These single-particle matrix elements can be found from angular momentum considerations and are shown in Table 1 of FFNII.

We follow FFN in using the single-particle result (eq. [19]) to estimate the total strength. Experimentally it is well established that the axial vector current is renormalized by a factor of $\sim(1/1.24)$ in nuclei. This results in a strength a factor of $(1/1.24)^2 \approx 1/2$ smaller than shell model calculations give. In addition, shell model calculations show that residual interaction-induced particle-hole correlations further reduce the total strength by a factor of 1 to a few. Typically, these correlations are more important for GT$^+$ transitions, so that the additional quenching is larger for these transitions. One way to incorporate the effects of quenching on the rates is through a tabulation of "effective logft-values" (Fuller et al. 1985). This allows users of the rates to determine when a given rate is dominated by experimentally determined low-lying transitions (and should not be quenched) and when a rate is dominated by an estimate of the GT resonance strength (and should be quenched). We do not follow this approach, but instead incorporate the

quenching by adopting a quenching factor of 4 for GT^+ transitions and 3 for GT^- transitions. These values for the quenching factors generally give strengths within a factor of 2 of more detailed strength determinations. When the quenched value for the strength is less than 1, we assign a configuration mixing strength of 1. As discussed below, this is roughly consistent with the results of (n, p) experiments for GT^+ blocked nuclei.

FFN estimated the centroid of the GT resonance by considering a zeroth-order shell model description for the spin flip part of the GT resonance. This configuration was compared with the zeroth-order shell model description of the daughter ground state and assigned an excitation energy

$$E_{\rm GT} = \Delta E_{\rm s.p.} + \Delta E_{\rm pair} + \Delta E_{\rm ph} \ . \qquad (20)$$

Here $\Delta E_{\rm s.p.}$ is the difference in single-particle energies between the two states (daughter ground state and spin flip GT resonance state), $\Delta E_{\rm pair}$ accounts for the difference in pairing energy between the two states, and $\Delta E_{\rm ph}$ (taken to be 2 MeV) accounts for the effects of configuration mixing and particle hole repulsion. For $T^> \rightarrow T^<$ transitions the energy of the IAS in the daughter is added to equation (20).

For the assignment of the GT centroids we adopt a procedure close to that outlined by FFN. However, as noted in the introduction, the FFN approach misses some important systematics in the centroids of the strengths as revealed by more recent experimental data and shell model calculations. One potential remedy for this is to do RPA or QRPA calculations for the strength distributions for nuclei too heavy to be studied via detailed shell model calculations. Such calculations have been done for a number of nuclei by several different groups. A simpler approach is to approximately account for the effects of the competition between the $k_{\sigma\tau}(\sigma_1 \cdot \tau_1)(\sigma_2 \cdot \tau_2)$ and $k_\tau(\tau_1 \cdot \tau_2)$ terms in the nuclear Hamiltonian. The effect of this competition on the centroid of the GT resonance is most easily seen in the Tamm Dancoff approximation from the argument given by Bertsch & Esbensen (1987). In this approximation the k_τ and $k_{\sigma\tau}$ forces give rise to a GT^- excitation energy scaling as

$$E_{\rm GT^-} \approx E_{\rm IAS} + \Delta E_{\rm so} + 2[k_{\sigma\tau} S_{\rm GT^-}/3 - (N-Z)k_\tau] \ . \qquad (21)$$

Here $\Delta E_{\rm so}$ is the spin orbit splitting characteristic of the single-particle transitions for the GT^- resonance. As an example of this equation, consider the case of ^{54}Fe and ^{56}Fe. The zeroth-order β^- strengths for these nuclei are $|M_{\rm GT}|^2 = 16.3$ (^{54}Fe) and 22.3 (^{56}Fe). For $k_{\sigma\tau} \sim (20/A)$MeV $\sim (2/3)$ k_τ, equation (21) implies $(E_{\rm GT^-} - E_{\rm IAS})_{^{56}{\rm Fe}} - (E_{\rm GT^-} - E_{\rm IAS})_{^{54}{\rm Fe}} \approx -1$ MeV. Shell model calculations and (p, n) experiments for these nuclei give this difference as approximately -2 MeV. As Fe becomes more and more neutron-rich $E_{\rm GT^-}$ approaches $E_{\rm IAS}$ and eventually falls below it (although perhaps beyond the neutron drip line for a nucleus as light as Fe).

A somewhat more sophisticated approach to incorporating the effects of the competition between the k_τ and $k_{\sigma\tau}$ forces is the random phase approximation with a separable force. In this approximation the GT^+ and GT^- resonances become eigenstates of the Hamiltonian. The energies of the resonances are approximately given by the roots of the algebraic equation

$$\frac{f_1}{\epsilon_i - \epsilon + \Delta^-_{\rm so}} + \frac{f_2}{\epsilon_i - \epsilon} + \frac{f_3}{-\epsilon_i + \epsilon + \Delta^+_{\rm so}} = -\frac{3}{2}\frac{1}{k_{\sigma\tau}}\frac{1}{S_{\rm tot}} \qquad (22)$$

(see Gaarde et al. 1981 for an application of this equation to experimentally observed β^- strengths, or Rowe 1970 for a more pedagogical discussion). In equation (22), $S_{\rm total} = S_{\rm GT^-} + S_{\rm GT^+} = 3|N-Z| + 2S_{\rm GT^+}$ is the sum of the strengths in the plus and minus directions, f_1 is the fraction of this strength in the GT^- spin-flip mode, f_2 is the fraction of this strength in the GT^- non–spin flip mode, and f_3 is the fraction of strength in the GT^+ direction. The spin orbit splittings $\Delta^+_{\rm so}$ and $\Delta^-_{\rm so}$ are the splittings appropriate for the spin flip transitions in the plus and minus directions, $\epsilon_i = (\epsilon_\pi - \epsilon_\nu)_i$ is the difference in the proton and neutron single-particle energies for the levels involved in the transition. The quantity ϵ_i is related to the energy of the IAS by $E_{\rm IAS} - \epsilon_i = 2k_\tau|N-Z|$. The largest root of equation (22) corresponds to the energy of the spin flip mode. Equation (22) reduces to equation (21) in the limit $f_1 = 1$.

Our approach for calculating the centroid of the GT^- resonance is based on equation (22). The strengths in this equation are estimated in the zeroth-order shell model picture described above. For consistency with FFN we take the spin orbit splittings from Seeger & Howard (see the table in Hillman & Grover 1969). When more than one spin flip transition contributes to the strength, we take the strength-weighted average. The parameter k_τ can be estimated using measured IAS energies and estimates for the particle-hole energies. Alternatively, an estimate for the IAS energy (eq. [17]) gives a relation between k_τ and ϵ_i. The parameter $k_{\sigma\tau}$ can be chosen to give good agreement with shell model and experimental results for the GT^- resonance in the *fp* shell. In this work we adopt $k_\tau = 28.5/A$ MeV and $k_{\sigma\tau} = 23/A$ MeV. These values are close to those given in Bertsch & Esbensen (1987) and Gaarde et al. (1981). It has previously been noted by a number of authors (e.g., Gaarde et al. 1981) that a simple prescription can do a fair job of predicting the centroids of the GT^- resonances (see Table 3). In Table 4 we reaffirm this by comparing the predictions based on equation (22) with measured and shell model results.

For the GT^+ resonance, estimates based on a separable force are not well justified. Higher order particle hole correlations and correlations induced by other terms in the Hamiltonian play a more important role. Nonetheless, the RPA result accounts for the spin orbit splittings and the systematics of the influence of the k_τ and $k_{\sigma\tau}$ forces in an approximate way. We estimate the centroid of the GT^+ resonance from the equation analogous to equation (22) (which is found by reversing the role of the plus and minus transitions, and by setting $\epsilon_i = (\epsilon_\nu - \epsilon_\pi)$ or alternatively by setting $\epsilon \rightarrow -\epsilon$ in eq. [22]). We also add an additional term to account for the effects of correlations missed by the separable force estimate:

$$E_{\rm GT^+} = E_{\rm GT^+,RPA} + \delta_{\rm ph} \ . \qquad (23)$$

A value of 2 MeV for the empirical correction $\delta_{\rm ph}$ gives good agreement with the results of experimental and shell model studies of nuclei in the lower half of the *fp* shell. This is demonstrated in Table 4.

Our simple estimate for $E_{\rm GT^+}$ probably breaks down as the *fp* shell approaches being filled. Fortunately, for most nuclei in this case ($A > 65$) the GT^+ transition is nearly blocked and there are indications that for such nuclei the GT^+ resonance strength can be simply approximated (see below). Likewise, for those proton-rich nuclei with substantial amounts of unblocked strength the electron capture

TABLE 3

COMPARISON OF THE SHELL MODEL GT^- CENTROIDS CALCULATED IN LMP WITH THOSE ESTIMATED FROM EQUATION (22) (PRESENT)

Parent Nucleus	LMP	Present
^{55}Fe	12.6	10.4
^{56}Fe[a]	9.6	8.5
^{57}Fe	12.6	11.5
^{58}Fe	11.0	9.5
^{59}Fe	13.6	12.6
^{60}Fe	10.3	10.6
^{61}Fe	13.8	13.75
^{62}Fe	11.8	11.7
^{58}Ni[a]	9.2	6.44
^{59}Ni	10.6	9.46
^{60}Ni[a]	9.0	7.5
^{61}Ni	13.3	10.6
^{62}Ni	9.2	8.2
^{63}Ni	13.2	11.5
^{64}Ni	9.6	9.15
^{65}Ni	12.	12.35
^{56}Co	13.2	12.7
^{57}Co	12.5	10.77
^{58}Co	14.7	13.7
^{59}Co	13.1	11.6
^{60}Co	14.0	14.8
^{61}Co	13.6	12.6
^{62}Co	15.3	13.9
^{63}Co	14.4	13.7
^{64}Co	16.0	16.7
^{65}Co	14.6	14.8
^{55}Mn	13.0	11.8
^{56}Mn	14.7	15.1
^{57}Mn	13.1	13.5
^{58}Mn	15.5	16.4
^{59}Mn	14.0	14.7
^{60}Mn	16.0	17.4
^{61}Mn	16.2	15.5

NOTES.—All energies are in MeV and refer to energy with respect to the daughter ground state. The shell model centroids in this table were taken from the tables or estimated from the graphs in Caurier et al. 1999 and LMP.

[a] For these nuclei the results from (p, n) experiments give a centroid approximately 0.7–1 MeV lower than the shell model results.

TABLE 4

COMPARISON OF THE SHELL MODEL GT^+ CENTROIDS CALCULATED BY LMP WITH THOSE ESTIMATED FROM EQUATION (23) (PRESENT)

Parent Nucleus	LMP	Present
^{55}Mn	4.6	4.6
^{56}Mn	5.9	6.4
^{56}Fe	2.6	2.4
^{56}Co	8.2	8.8
^{58}Mn	5.5	5.15
^{58}Co	7.35	8.1
^{58}Ni	3.75	3.65
^{59}Co	5.05	5.0
^{60}Co	6.35	6.74
^{60}Ni	3.4	2.7
^{61}Fe	2.1	1.8
^{61}Co	3.7	3.4
^{61}Ni	4.7	4.7
^{61}Cu	6.7	6.4
^{62}Ni	2.1	1.8
^{64}Ni	1.3	1.8

NOTES.—All energies are in MeV and refer to energy with respect to the daughter ground state. The shell model centroids in this table were also taken from Caurier et al. 1999 and LMP. Where an experimental result is listed along with the shell model result we have presented the experimental result.

Q-value is large, so again the rate is not terribly sensitive to assumptions about the centroid. For the few proton-rich nuclei with modest GT^+ strength, we can compare our results to the more detailed QRPA calculations of Sarriguren, de Guerra, & Escuderos (2001). These authors performed QRPA studies for even-even Ge, Se, Kr, and Sr isotopes. For the most part their calculated electron capture half-lives agree well with experimental half-lives.

For ^{66}Ge, ^{68}Ge, and ^{70}Se, Sarriguren et al. (2001) find that the strength distribution is not very sensitive to which of two nearly degenerate shapes the nucleus assumes, so that a direct comparison with our estimate is sensible. For these nuclei our estimate for the centroid of the resonance is lower than theirs by 1.5 MeV (^{66}Ge), 1.8 MeV (^{68}Ge), and 2.5 MeV (^{70}Se). For some of these nuclei it is not clear which estimate is correct. Sarriguren et al. (2001) show that their method gives a centroid about 2 MeV higher than the experimental centroid for ^{54}Fe and ^{56}Fe and that there calculation for ^{70}Ge misses a modest amount of experimentally determined low-lying strength.

However, in at least one case (^{70}Se), our assignment of the strength is at least 0.5–1 MeV too low. We know this because a calculation of the ground state lifetime based on our estimate for the strength distribution is about 2 times shorter than the experimentally determined half-life. (As discussed above, though, we use experimental information in place of other estimates when an experimentally determined half-life is available.) We will argue in the last section that the uncertainty in the placement of the centroid of the GT^+ strength is not very important for nuclei in the mass range we are considering.

As the GT^+ strength decreases (i.e., as an isotope becomes more neutron rich), equation (23) eventually gives a negative excitation energy for the resonance in the daughter. This typically happens when the single-particle estimate for the strength (eq. [19]) is less than about 5. In this case, the strength is dominated almost entirely by configuration mixing. There are a few (n, p) studies of such nearly blocked nuclei. Vetterli et al. (1992) studied ^{70}Ge(n, p)^{70}As and ^{72}Ge(n, p)^{72}As. The experimentally determined GT strength for ^{70}Ge is $B(\mathrm{GT}) = 0.84 \pm 0.13$ or $B(\mathrm{GT}) = 0.72 \pm 0.14$. The two different values correspond to different ways of estimating the $\Delta L = 0$ component of the (n, p) cross section. The higher estimate comes from a multipole decomposition (m-d) of the cross section, while the smaller estimate is derived by approximating the cross section measured at 5°.8 as the $\Delta L = 1$ component of the cross section. For the m-d the strength distribution for ^{70}Ge is approximately flat up to a few tens of MeV in excitation energy in ^{70}As. For the 5°.8 subtraction method, the strength falls after about 6 MeV in excitation energy in ^{70}As. For ^{72}Ge $B(\mathrm{GT}) = 0.23 \pm 0.05$ (5°.8) or $B(\mathrm{GT}) = 0.86 \pm 0.14$ (m-d) and the strength distribution is roughly flat or falls off after about 6 MeV

depending on the background subtraction method. Helmer et al. (1997) have studied ^{76}Se$(n, p)^{76}$As. They find $B(\mathrm{GT}) = 1.45$ with a roughly flat strength distribution for the m-d method, and $B(\mathrm{GT}) = 0.35$ with a strength extending to about 6 MeV in ^{76}As if the 6° data are used to estimate the $\Delta L = 1$ component of the cross section. In this work we adopt the procedure that when the RPA estimate $E_{\mathrm{GT}^+,\,\mathrm{RPA}}$ appearing in equation (23) is negative with respect to the daughter ground state, or when the GT^+ strength in the zeroth-order shell model picture is zero, the strength distribution is represented by a 1 MeV-width Gaussian centered at 1.8 MeV. This is approximately consistent with the experimental data analyzed using the 5°.8 (6°) background subtraction method. Our prescription misses the high-lying strength estimated from the experimental data analyzed using the multipole decomposition method. We will discuss in the last section the uncertainties in the rates resulting from the unknown strength distribution for these blocked nuclei.

5. THERMAL CONSIDERATIONS

The picture for Fermi and Gamow-Teller strengths outlined above becomes more complicated at high temperatures on account of the thermal population of parent excited states. In evaluating the contribution to the rates of transitions between low-lying levels, we use the same set of experimentally determined levels discussed above.

As the temperature rises, the evaluation of equation (1) requires knowing the strength distributions of an impossibly large number of states. For example, at a temperature of 1 MeV the partition function for an odd-odd nucleus with $A \approx 60$ is a few hundred, and the mean excitation energy is $T^2\rho_{\mathrm{F}} \approx T^2A/8 \approx 7$ MeV (here $\rho_{\mathrm{F}} \approx a$ is the level density at the Fermi surface and $a \approx A/8$ is the level density parameter). The approximation traditionally (see FFNII) used to make the problem tractable is the Brink approximation, which postulates that the centroid of the Gamow-Teller strength distribution corresponding to a parent state at excitation energy E_i is shifted up by an energy E_i with respect to the centroid of the strength distribution corresponding to the parent ground state. It is generally assumed that the total strength remains the same for all transitions. The validity of the Brink approximation has been investigated in some detail by LMP. They find that the approximation is good for the first few low-lying states for which they calculate strength distributions.

With the Brink approximation, the contribution of discrete state to high-lying resonance state transitions can be approximated. For definiteness we assume in the following discussion that the parent nucleus has isospin $T^>$, the daughter nucleus has isospin $T^<$, and that the GT^- operator acting on the parent generates states in the daughter (and conversely). Each parent state ($|\psi_i^{\mathrm{P}}\rangle$) has a corresponding Fermi resonance ($|F_i\rangle = T^-|\psi_i^{\mathrm{P}}\rangle$) and collective Gamow-Teller resonance ($|\mathrm{CGT}_i\rangle = \mathrm{GT}^-|\psi_i^{\mathrm{P}}\rangle$) in the $T^<$ daughter. With the Brink approximation, the Q-values for these transitions are independent of the excitation energy of the thermally populated parent state. The overall transition rate for these processes can be obtained from a calculation of the ground state rate alone, but with the population factor of the ground state set to unity. This is part of the "FFN trick."

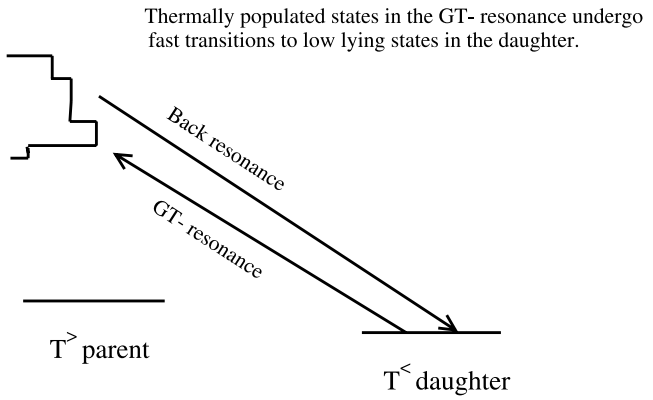

FIG. 4.—Illustration of the position and energetics of discrete state-resonance transitions (back resonances).

Likewise, it is possible to thermally populate the collective Gamow-Teller states in the $T^>$ parent ($|\mathrm{CGT}_j\rangle = \mathrm{GT}^+|\psi_j^{\mathrm{D}}\rangle$). These thermally populated states can decay to the daughter with large overlap. These "back resonances" are shown in Figure 4. Suppose for a moment that the GT^+ resonance corresponding to a state in the daughter is confined to a single state in the parent. In this case the Brink approximation implies that for each state with excitation energy $E_{\mathrm{daughter},\,j}$ in the daughter, there is a corresponding GT^+ resonance state ($|\mathrm{CGT}_j\rangle = \mathrm{GT}^+|\psi_j^{\mathrm{D}}\rangle$) in the parent with excitation energy $E_0 + E_{\mathrm{daughter},\,j}$. Here E_0 is the excitation energy in the parent of the resonance state corresponding to the daughter ground state. Because in the Brink approximation the Q-values and strengths for all the transitions $(E_0 + E_j)_{\mathrm{parent}} \rightarrow (E_j)_{\mathrm{daughter}}$ are the same, the rate contribution for each transition is also the same and can be written as $\bar{\lambda}$. The contribution of the back resonances to the rates can be directly evaluated:

$$\begin{aligned}\lambda_{\mathrm{backres}} &= \frac{\bar{\lambda}\sum_i \exp(-E_{\mathrm{parent},\,i}/T)(2J_{\mathrm{parent},\,i}+1)}{Z_{\mathrm{parent}}} \\ &\approx \frac{\bar{\lambda}\sum_j \exp(-E_{\mathrm{daughter},\,j}+E_0)/T)(2J_{\mathrm{daughter},\,j}+1)}{Z_{\mathrm{parent}}} \\ &= \bar{\lambda}\exp(-E_0/T)\frac{Z_{\mathrm{daughter}}}{Z_{\mathrm{parent}}}\ . \end{aligned} \tag{24}$$

Equation (24) was first derived in FFNII and is sometimes referred to as the "FFN trick."

In this work we represent the resonance strength distribution by a Gaussian of nominal width σ. For the GT^+ strength distribution we take $\sigma = 1$ MeV and for the GT^- strength distribution we take $\sigma = 2$ MeV. This approximation does not fairly represent the complex structure and variation seen in real strength distributions. However, we will see in the last section that this simple approximation captures the features relevant for calculations of weak rates in a stellar environment. The case where the resonance is spread over several states in the parent can be treated similarly to the case where the resonance is concentrated in a single state. If the resonance corresponding to the ground state in the daughter is spread over states with excitation energy $E_0, E_1, \ldots, E_n$ in the parent, with corresponding rates to the daughter ground state given by $\bar{\lambda}_{0j}$, then equation (24)

becomes

$$\lambda_{\rm backres} \approx \frac{\sum_j \bar{\lambda}_{0j} \exp(-E_{0j}/T) Z_{\rm daughter}}{Z_{\rm parent}} \ . \qquad (25)$$

Apart from spin weighting corrections, this equation is exact in the limit where the Brink approximation holds (i.e., the strength distribution from every daughter state is identical to the strength distribution from the daughter ground state except for an overall shift in energy).

The interesting feature of equation (25) is that if all of the Q-values for the n states are comparable (so that the E_{0j}/T are all comparable), then

$$\lambda_{\rm backres} \approx n\langle\bar{\lambda}_{0j}\rangle \exp(-E_0/T) Z_{\rm daughter}/Z_{\rm parent} = \bar{\lambda} \exp(-E_0/T) Z_{\rm daughter}/Z_{\rm parent} \ , \qquad (26)$$

independent of n. Here the relation $n\langle\bar{\lambda}_{0j}\rangle \approx \bar{\lambda}$ (where $\bar{\lambda}$ is the rate of decay calculated assuming that the GT resonances are confined to single states) holds because the total strength in the GT resonance is independent of the number of states it is spread over. In a sense equation (26) is counterintuitive because one might expect that if the strength is spread out over n states in the parent, the decay rate from the parent should be a factor of $1/n$ smaller. However, in some cases the strength distributions arising from different states in the daughter must overlap (i.e., correspond to identical states in the parent) to the extent that the level densities in the parent and in the daughter are comparable. This is accounted for by the ratio of partition functions appearing in equation (25). As discussed above, equations (24) and (26) represent the limiting form of equation (25) and are only valid when the width of the GT back resonance is small compared to the temperature and typical decay Q-value. When these conditions are not met, more detailed information (e.g., from shell model calculations) about the strength distribution is needed and can be incorporated in equation (25). In turn, equation (25) is only appropriate when variations in the back resonances corresponding to different daughter states are small (apart from the overall shift in energy of the centroid described by the Brink hypothesis).

In principal, equation (25) is not needed, and the rates can be estimated through a direct shell model calculation of the strength distribution from daughter states. To illustrate potential difficulties associated with such an approach consider the definite example of the β-decay of Mn to Fe (we shall consider $A = 56$ for illustration). For simplicity, suppose that (i) the width of the GT+ resonances in Mn (generated by applying GT$^+$ to states in Fe) are small compared to the temperature as well as the Q-value for decays from these states and (ii) the partition functions for Mn and Fe are identical ($Z_{\rm Mn} = Z_{\rm Fe}$). In the limit where the Brink approximation holds, the β-decay rate of Mn is approximately $\bar{\lambda}\exp(-E_0/T)$, where the symbols have the same meaning as in equation (24). We now want to compare this decay rate to the decay rate calculated in a Lanczos-based approach. For simplicity suppose first that, apart from the ground state, the only states considered in Mn are those calculated to comprise the GT$^+$ strength distribution of the ground state of Fe. The partition function calculated in this approach is $Z_{\rm Mn} = [7 + 3m_{\rm Lan}\exp(-E_0/T)]$, where $m_{\rm Lan}$ is the number of Lanczos iterations done for the GT+ strength of the Fe ground state, the number 7 arises because the ground state spin of ^{56}Mn is 3, and the number 3 arises because states in Mn connected to the (0^+) ground state of Fe via allowed GT transitions have $J = 1$. The calculated β-decay rate of Mn is then $3\bar{\lambda}\exp(-E_0/T)/[7 + 3m_{\rm Lan}\exp(-E_0/T)]$. The dependence on $m_{\rm Lan}$ does not cancel out. The calculated decay rate is a function of how many Lanczos iterations are done. If $E_0/T < 1$, then the decay rate that is calculated if 100 iterations are done ($m_{\rm Lan} = 100$) is of order a factor of 30 smaller than the decay rate that is calculated if only one Lanczos iteration is done. Provided that the states in the GT strength distribution can be converged, the dependence of the calculated decay rate on $m_{\rm Lan}$ can be partly alleviated by considering the strength distributions corresponding to many daughter excited states. We note that LMP used detailed calculations of strength distributions (and did not simply factor out an average matrix element as in the simple example presented here) in their calculations of β-decay rates.

To show how differences in the treatment of partition functions can influence estimates of high-temperature β-decay rates, we plot in Figure 5 a comparison between our calculated β^--decay rates and those of LMP at a temperature of $T_9 = 30$ and a density of $\rho Y_e = 10$ g cm^{-3}. These thermodynamic conditions are artificial but serve the purpose of illustration. When the β-decay rate is fast (and insensitive to the finer details of the strength distribution), the discrepancy between the two calculations is about a factor of 10. From our simple analysis it is not clear that either set of rates is more reliable. However, it is clear that differences in treatments of the partition functions can result in significant differences in estimates of the rates.

The trend of greater disagreement with faster decay rate seen in Figure 5 arises from the competition of two factors. For low decay rates, the Q-value of the decay (excitation energy of the GT$^+$ resonance with respect to the daughter ground state), is typically small. In this case the width of the

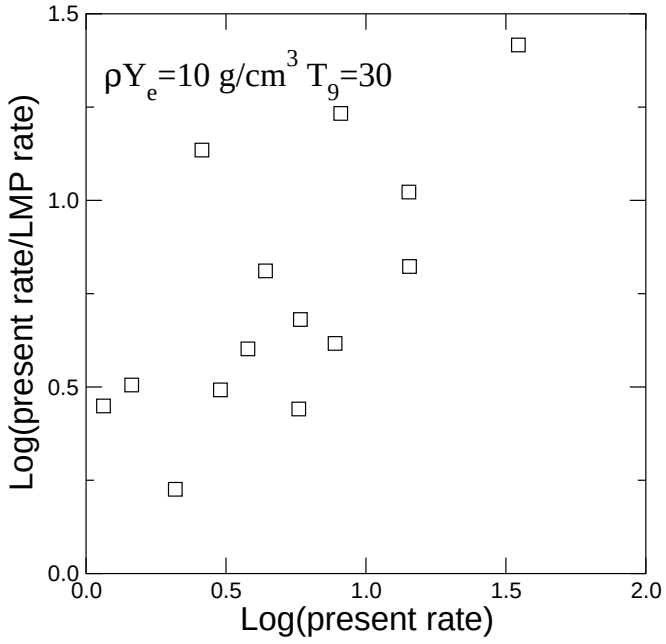

FIG. 5.—Comparison of our β^--decay rates with the LMP rates for nuclei in the mass range $A = 60$–65. The comparison is made at $T_9 = 30$, $\rho Y_e = 10$ g cm^{-3}. These conditions are artificial but serve to illustrate the influence of the treatment of the partition function on estimates of the weak rates. In all plots where a rate is shown the rate is in units of s^{-1}.

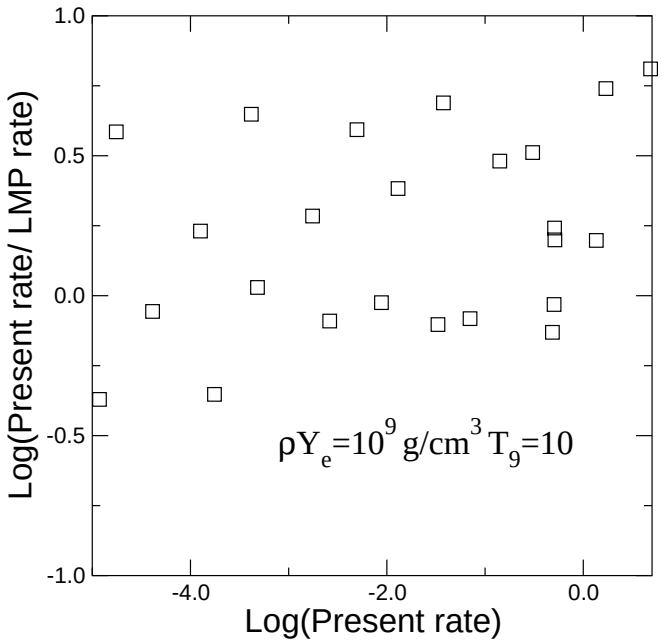

FIG. 6.—Same as Fig. 5, but at $T_9 = 10$, $\rho Y_e = 10^9$ g cm^{-3}, conditions approximating the post Si burning degenerate core before collapse.

resonance enhances the decay rate compared to the decay rate calculated from our artificially narrow resonance. For faster decay rates, the Q-value is large, the lifetime is relatively insensitive to the width of the resonance, and the LMP estimate differs from the present estimate mostly because of differences in estimates of the partition function.

The effect, and the importance of consistency in partition functions in general, can be illustrated by considering the conditions in the post–silicon burning, precollapse core of a massive star. There electron capture proceeds on iron peak nuclei, driving them to a neutron excess where "reverse" β^--decay balances "forward" electron capture. For example, Aufderheide et al. (1994) identify ^{64}Cr as the end-point nucleus where the forward and reverse neutronization rates balance. In balanced conditions, partition functions are crucial rate and abundance determinants. We can compare our rates with LMP as in Figure 5, but now for $T_9 = 10$, $\rho Y_e = 10^9$ g cm^{-3}, roughly approximating immediately precollapse conditions. This comparison is shown in Figure 6. Again there is a systematic trend: the LMP rates are lower than ours by a factor of 4 on average with a fair scatter. This is smaller than the disagreement presented above for the fastest β-decay rates, but still of potential significance given the dependence of the initial Fe core mass on the electron fraction. Part of the discrepancy between the rate estimates undoubtedly stems from differences in placement and width of GT strength and other nuclear uncertainties.

However, the partition effect outlined above likely plays a role as well. In fact, these conditions ($T_9 = 10$, $\rho Y_e = 10^9$ g cm^{-3}) are electron degenerate with Fermi energies $\sim$5 MeV, precluding significant β-decay for all but the nuclear decay pairs with relatively large Q-values, just those where we argued that the partition function-based uncertainties in rate estimates could be large.

In evaluating the ratio $Z_{\rm daughter}/Z_{\rm parent}$ in equation (25) we use the compilation of partition functions from Rauscher & Thielemann (2000). These partition functions include experimentally determined low-lying levels and are supplemented at higher excitation energies by a level density calculated from a back shifted Fermi gas formula. It should be noted that, in addition to well-known difficulties with estimating partition functions, some error may be introduced by the use of parameterized partition functions. At low temperatures the partition functions of Rauscher & Thielemann (2000) agree well with the partition functions we calculate for evaluating the rates between low-lying levels. For temperatures above 2 MeV we take $Z_{\rm daughter}/Z_{\rm parent} = 1$. This is valid because the mean excitation energy at these temperatures is well above the pairing gap.

We do not claim that our partition function treatment is necessarily better than others, and it may well be inadequate in some conditions. In fact there is a basic inconsistency in our rates: we include many states in our partition function sums for which we include no weak interaction strength. Ideally, we should include all states and all associated weak strength: only fully converged Lanczos and Monte Carlo calculations of weak strength and partition functions currently do this.

Failing to estimate partition functions and strength functions consistently can lead to inaccurate predictions of final *equilibrium* parameters. In equilibrium, the hard-won rates no longer matter and only the partition functions govern the final quantities of interest (Y_e, abundances, etc.).

6. RESULTS AND DISCUSSION

6.1. *A Validity Test: Comparison with Shell Model Based Rates for A = 60–65*

Here we address the reliability of our calculated rates. We have shown in § 3 that with a simple prescription some gross features of the strength distribution, in particular the total strength and centroid of the distribution, may be estimated. However, shell model and experimental results typically show a rich structure in the strength distribution, with this structure varying markedly from nucleus to nucleus (e.g., Caurier et al. 1999). Do the rates depend sensitively on the finer features of the strength distribution? Or, alternatively, can a computationally simple method give a good estimate of the weak interaction rates? These questions can be addressed by comparing our relatively simply derived rates with rates based on more detailed large dimension shell model calculations.

In Figures 7 and 8 we show the log of the ratio of our calculated β-decay rates to those calculated in Langanke & Martinez-Pinedo (2000) at several temperature/density points relevant for stellar collapse, and for all nuclei in the range $A = 60$–65 for which LMP calculated rates. Note that these figures are for quite low temperatures, $T_9 = 3$ and 5, respectively, so that the thermal population of the back resonance plays a negligible role in determining the decay rate. Consequently, the rates calculated by LMP at these temperatures should be essentially exact. The horizontal axis in this figure is the log of the β-decay rate calculated by LMP. We have presented the comparison in this way because nuclei with very small rates will not be so important in determining the evolution. The comparison is generally remarkably favorable, with typical results differing by less than a factor of 2. Figures 9, 10, and 11 are the same as the previous three figures, but now electron capture rates are being compared.

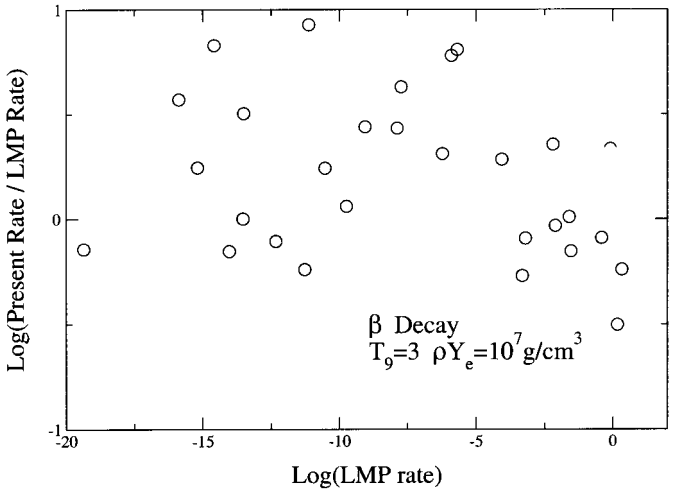

FIG. 7.—Comparison of our β-decay rates calculated using a simple estimate of the strength distribution with the more sophisticated calculations of Caurier et al. (1999) and Langanke & Martinez-Pinedo (2000). The different circles correspond to different nuclei. Comparisons for all nuclei in the mass range $A = 60$–65 for which Langanke & Martinez-Pinedo provide rates are presented. Here $T_9 = 3$ and $\rho Y_e = 10^7$ g cm^{-3}.

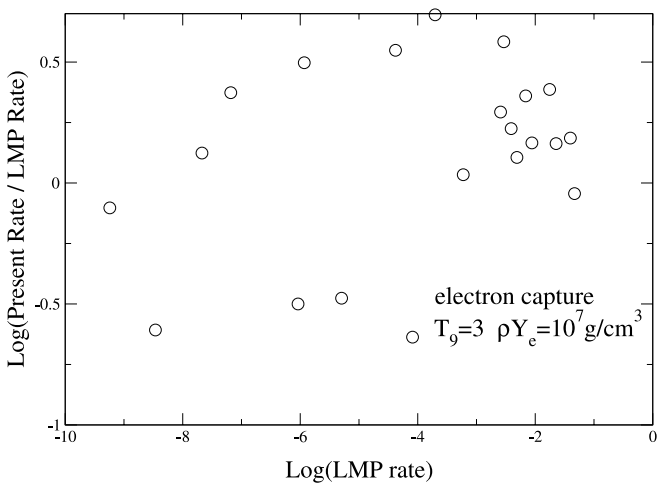

FIG. 9.—Comparison of our electron capture rates with those of Langanke & Martinez-Pinedo at $T_9 = 3$, $\rho Y_e = 10^7$ g cm^{-3}. Only results for nuclei that are estimated by LMP to have electron capture rates larger than 10^{-10} s^{-1} are shown.

Again, the comparison is favorable, the rates as calculated in the two schemes being within a factor of 3 or so. This is surprising given the potential sensitivity of electron capture rates to the placement and the width of the Gamow-Teller distribution.

The fact that a simple prescription and rough estimates of the strength do a reasonably good job in getting the rates relevant for stellar collapse is not to say that all rates are accurately determined at all temperatures and densities with a simple model. Some of our calculated rates deviate significantly from more detailed calculations. This typically occurs for $\beta^-(\beta^+)$-decay when the rates are exponentially sensitive to the placement of a resonance, or for lepton capture when the maximum lepton energies are just on the edge of being able to reach the resonance in the daughter. Typically, this exponential sensitivity is accompanied by a very small rate, so that it is not very important for stellar evolution.

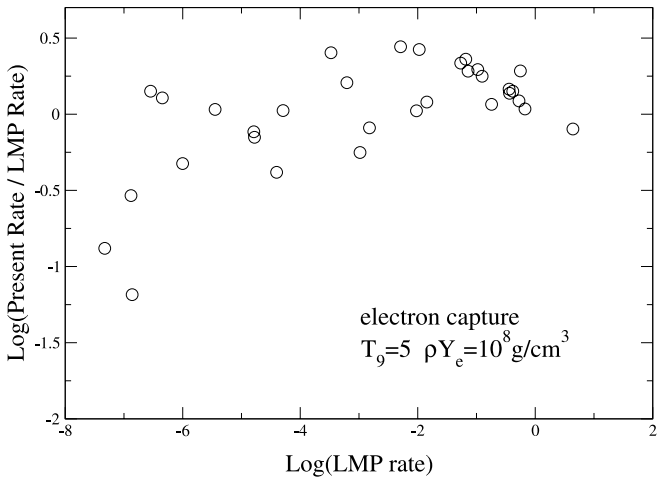

FIG. 10.—Same as Fig. 9, but at $T_9 = 5$ and $\rho Y_e = 10^8$ g cm^{-3}

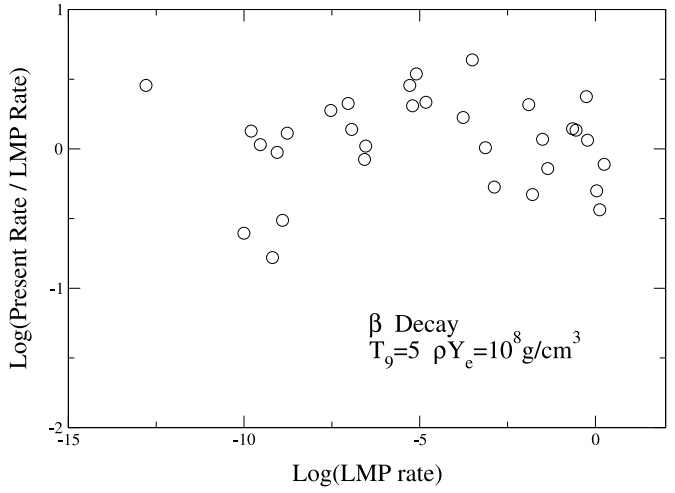

FIG. 8.—Same as Fig. 7, but with $T_9 = 5$ and $\rho Y_e = 10^8$ g cm^{-3}

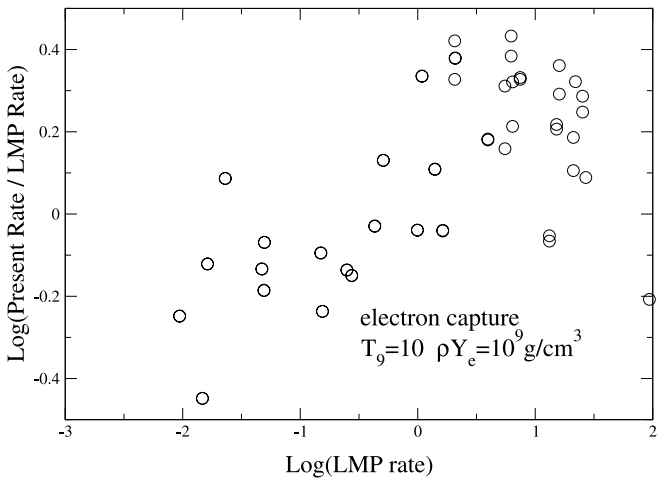

FIG. 11.—Same as Fig. 9, but at $T_9 = 10$ and $\rho Y_e = 10^9$ g cm^{-3}

6.2. *Examples of Some Rates Important in X-Ray Burst Environments*

X-ray bursts arise from the thermonuclear burning of hydrogen and helium accreted onto the surface of a neutron star in a binary system (see Wallace & Woosley 1981). Characteristic temperatures during burning are a few hundred keV, and characteristic densities are $\rho Y_e \approx 10^6$ g cm^{-3}. The creation of nuclei heavier than $A \approx 40$ occurs via the *rp*-process, in which nuclei undergo (p, γ) reactions until they approach the proton drip line and/or β^+/ec-decay intervenes. The time for burning along the *rp*-process path is set to some extent by the β^+/ec lifetime of a few important waiting point nuclei. Here we present a few examples of important rates.

Three important waiting point nuclei with $A < 80$ are the even-even (proton bound) nuclei ^{64}Ge, ^{68}Se, and ^{72}Kr (Schatz et al. 2001). For each of these nuclei the single-proton capture daughter $(Z + 1, N)$ is unbound, while the next heaviest isotone $(Z + 2, N)$ is bound. At low temperatures ($T_9 \lesssim 1.5$) the weak rate most important for determining flow toward the valley of β stability is $\lambda_{\beta^+}(Z, N)$. For higher temperatures an equilibrium between (Z, N) and $(Z + 2, N)$ is reached, so that $\lambda_{\beta^+}(Z + 2, N)$ is also important. As a typical example we discuss $^{72}_{36}$Kr and its two-proton capture daughter $^{74}_{38}$Sr.

The first 2^+ excited state of ^{72}Kr lies at $\approx$700 keV and is not significantly populated for temperatures $T_9 < 2.5$. At $T_9 = 3$, the thermal population of the first 2^+ state increases the β^+ rate by about 25%. The ground state lifetime of ^{72}Kr is experimentally determined. The low-lying strength distribution in the daughter (^{72}Br) has also been measured. With the ground state lifetime and low-lying strength distribution measured, the only missing piece of information is the strength distribution at excitation energies too high to be experimentally observed. Our rough estimate (eq. [23]) places a portion of the resonance strength within the Q-value window for the decay. In order not to conflict with the experimentally determined lifetime we push this strength up to $Q = 0$ in our calculation.

To quantify the uncertainty in the rates arising from the high-lying resonance strength we plot in Figure 12 the total rate ($\beta^+ + ec$) for ^{72}Kr as a function of density and at zero temperature. Also included in this figure is the fraction of the total rate coming from $Q = 0$ and above. The figure indicates that the experimentally determined lifetime is sufficient for a determination of the low-temperature decay rate at the few percent level for $\rho Y_e < 10^6$ g cm^{-3}. At $\rho Y_e = 10^7$ g cm^{-3}, our simple estimate shows the high-lying strength accounting for $\sim$15% of the total weak rate. Because our method puts essentially all of the strength at $Q = 0$, and very little above $Q = 0$, it is unlikely that we have underestimated the contribution to the rate from the high-lying resonance strength.

The decay of ^{74}Sr is more easily calculated because the ground state (or a low-lying excited state) of the odd-odd $N = Z$ daughter (^{74}Rb) is the IAS of the ground state of ^{74}Sr. The large matrix element and Q-value ($\sim$10 MeV) for the Fermi decay mean that electron capture cannot compete with β^+-decay in X-ray burst conditions for this case. It is difficult to reliably estimate the contribution to the β^+ rate from GT$^+$ transitions, but a reasonable estimate is that the diffuse GT$^+$ strength only decreases the ground state lifetime by at most 10%–20%.

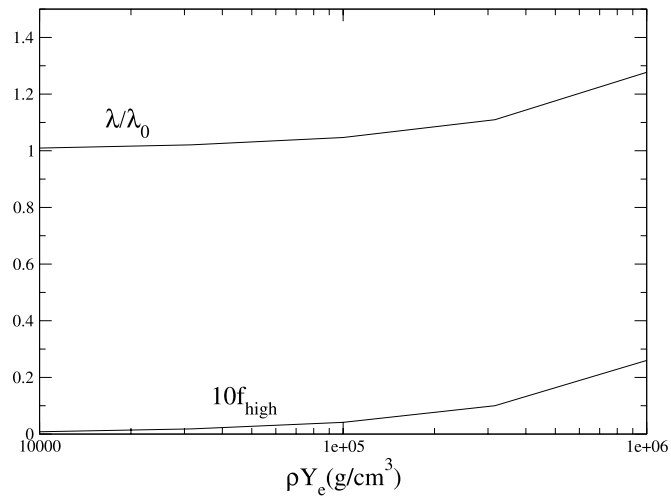

FIG. 12.—Influence of high-lying resonance strength on the total rate ($\beta^+ + ec$) for ^{72}Kr. In this figure $f_{\rm high}$ is an estimate of the fraction of the total rate arising from transitions involving experimentally unmeasured, high-lying resonance strength. The upper curve, labeled λ/λ_0, shows the ratio of the total rate to the β^+-decay rate. All rates shown in this plot are calculated at zero temperature.

By mirror symmetry, a low-lying thermally populated state of ^{74}Rb corresponds to an IAS in the next even-even β^+ nucleus (^{74}Kr), so that the chain ^{74}Sr $\rightarrow$ ^{74}Rb $\rightarrow$ ^{74}Kr is fast and dominated by Fermi transitions. The decay of the odd-odd $N = Z$ nucleus (^{74}Rb in this example) should be calculated as the decay of a thermally populated back resonance as discussed above. This is because only those parent states with an IAS in the even-even daughter nucleus decay via the Fermi transition. Since the partition function of the odd-odd parent increases more rapidly with temperature than the partition function of the even-even daughter, the decay rate decreases rapidly with increasing temperature. Another set of nuclei important for the *rp*-process with decays dominated by the Fermi transitions are those nuclei with $(Z = N + 1,\ N = \text{even})$. These have an IAS near or at the ground state of the β^+ daughter.

During *rp*-process burning, the temperature and electron Fermi energy are too low for electron capture to efficiently compete with β^+-decay for near-proton drip line nuclei characterized by large decay Q-values. Therefore, for these nuclei the thermal lifetime can be reliably estimated from the β^+-decay rate, and electron capture is not so important. By contrast, nuclei closer to the valley of stability have smaller Q-values and their lifetimes are nearly entirely determined by continuum electron capture.

For example, consider ^{66}Ge, a nucleus important in steady state burning on and/or near neutron star surfaces. This nucleus has a Q-value of only $\sim$2 MeV and a fair portion of the weak strength lies at the upper end of the Q-value window. Consequently, thermal electron capture dominates over positron decay for $\rho Y_e \gtrsim 10^5$ g cm^{-3}. This is shown in Figure 13.

6.3. *Weak Rates in the Late Time Presupernova Star*

Here we discuss some of the systematics of the weak rates in the hot and electron-degenerate core during the $\sim 10^4$ s before core bounce. Most of the nuclei with $A > 65$ present in the core will be blocked or nearly blocked to GT$^+$

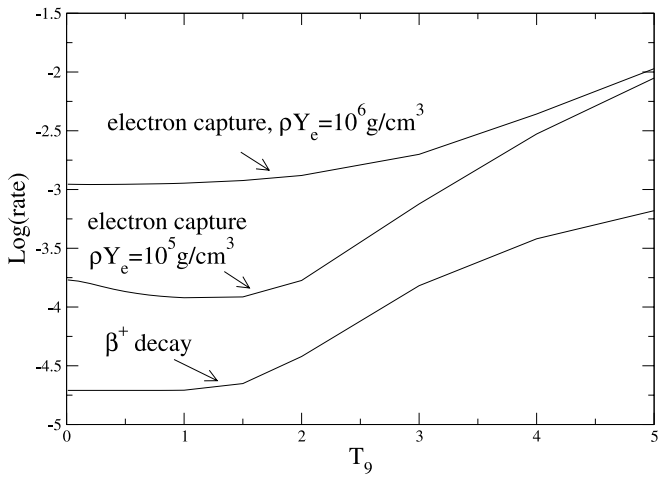

FIG. 13.—β^+/ec rates for ^{66}Ge. The increase of the β^+ rate with temperature arises from the fast decay of the thermally populated first $J^\pi = 2^+$ excited state. Unlike the 0^+ ground state, the 2^+ state can have allowed transitions to several 2^+ and 3^+ daughter states. The decrease in the electron capture rate at low temperatures is likely an artifact of our calculation and arises because the 0^+ ground state has substantial GT strength at high daughter excitation energies. As the daughter level structure is poorly known at these high excitation energies, our calculation does not include estimates of the allowed matrix elements for the decay of the first excited 2^+ state to those states.

transitions in the zeroth-order shell model picture. Our calculation of the electron capture rates for these nuclei is based in part on an estimate of the configuration mixing modification of the GT$^+$ strength and energy distribution. In particular, we model the GT$^+$ strength for blocked nuclei as a 1 MeV Gaussian of unit total strength centered at 1.8 MeV in the daughter. Forbidden transitions and transitions allowed by the thermal unblocking of strength will also contribute to the electron capture rates. It is useful to estimate how large the configuration mixing strength must be in order to justify the neglect of these latter types of transitions.

Thermal unblocking (Fuller 1982) refers to the opening at finite temperature of allowed transitions that would otherwise be disallowed (blocked) at zero temperature. If the strength distributions for all daughter→parent transitions were known, then thermal unblocking could accurately be treated as the population of the GT$^-$ back resonances described above. This is because detailed balance implies that the matrix element for a transition in one direction is the same as the matrix element for the transition in the opposite direction. Thinking about the thermal unblocking problem in this way suggests that for $T \lesssim 2$ or 3 MeV thermal unblocking is unlikely to be important in the SN environment—the centroid of the GT$^-$ resonance is typically at 10 MeV or higher for these nuclei, so that only the tail of the GT$^-$ resonance can be significantly populated.

A consideration of thermal unblocking in terms of the structure of low-lying levels is also useful. Assume that parent states with zeroth-order shell model configurations allowing GT$^+$ transitions comprise a fraction δZ of the total partition function. Then, an effective thermal unblocking matrix element is $|M_{\rm TU}|^2 \approx (\delta Z/Z)|M_{\rm sp}|^2$. Here $|M_{\rm sp}|^2 \approx 1-3$ is a typical single-particle allowed transition matrix element. An accurate estimate of δZ is very difficult and an important open issue. Fuller (1982) parameterizes $\delta Z \approx Z\exp(-E^*/T)$, with E^* the excitation energy of the lowest parent excited state with an allowed GT$^+$ transition in the zeroth-order shell model picture. With this schematic notation, thermal unblocking can compete with a configuration mixing strength of 0.1–1 if $E^*/T \lesssim 2$. For a typical $E^* \sim 5$ MeV, then, thermal unblocking can be neglected for $T \lesssim 2$ MeV. for $T > 2$ MeV the thermal population of the GT$^-$ resonance states (which we do include in our calculations) also becomes important.

Forbidden transitions become important as the electron chemical potential increases and the wavelength of the leptons involved in an electron capture event become small enough to probe structure in the nucleus. Again following the convention of Fuller (1982), the contribution to the electron capture rate from forbidden transitions can be written as $\lambda_{\rm for} \sim |M_{\rm for}|^2 f_{\rm for}(E_{\rm for},\ Q,\ \mu_e)$. Here $|M_{\rm for}|^2 \sim 10$–20 is roughly the number of protons in the *fp* shell multiplied by a typical single-particle first forbidden matrix element. The unique first forbidden phase space factor $f_{\rm for}$ depends on the centroid in energy of the forbidden strength distribution $E_{\rm for}$, the parent-daughter mass difference Q, and the electron chemical potential μ_e. For a typical $Q = 10$ MeV, forbidden transitions compete with a low-lying configuration mixing strength of $\sim 1/2$ for $\mu_e = 31$ MeV if $E_{\rm for} = 5$ MeV. If the centroid of the forbidden strength lies instead at $\sim$10 MeV above the daughter ground state, then forbidden transitions do not become important until $\mu_e > 37$ MeV. These conclusions are in rough agreement with the detailed calculations of Langanke, Kolbe, & Dean (2001) for the contribution of forbidden transitions and thermal unblocking to the electron capture rates.

With the assumption that the high-density electron capture rates are dominated by transitions involving low-lying configuration mixing strength, these rates are trivial functions of the electron Fermi energy and the parent-daughter mass difference. This is shown in Figure 14, where the electron capture rates are presented for nuclei with $(N-Z)/A > 0.1$ and $65 < A < 81$. The dependence of the rate on the Q-value for the transition is given by the simple analytic

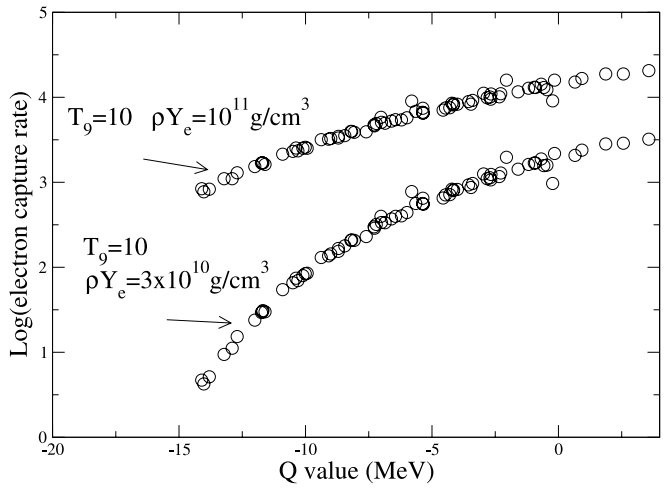

FIG. 14.—Electron capture rates for nuclei in the mass range $65 < A \leq 80$ and for which $(N-Z)/A > 0.1$ as a function of the Q-value (defined here as the parent-daughter atomic mass difference). These rates have a simple dependence on the Q-value (see eq. [27]) because of our assumption that the configuration mixing strength is nucleus-independent for GT$^+$ blocked nuclei.

expression

$$\lambda \approx 2\ln(2)10^{-3.6}(kT/m_ec^2)^5|M_{\rm GT}|^2 \times \left[F_4(\eta_{\rm eff}) + \bar{q}^2F_2(\eta_{\rm eff}) + 2\bar{q}F_3(\eta_{\rm eff})\right] . \quad (27)$$

Here $\eta_{\rm eff} = (U_{\rm F} + m_ec^2 + q - E_{{\rm res},d})/kT$, with $E_{{\rm res},d}$ the centroid of the GT^+ resonance in the daughter, $q = (M_p - M_d)c^2$, $\bar{q} = |q - E_{{\rm res},d}|/kT$, and the extra prefactor of 2 approximately accounts for the Coulomb distortion of the incoming electron for nuclei with $Z \approx 30$–40. This equation assumes that $q - E_{{\rm res},d}$ is negative. The functions

$$F_k(\eta) = \int_0^\infty \frac{x^k dx}{e^{x-\eta} + 1} \quad (28)$$

appearing in equation (27) are the relativistic Fermi integrals. Setting $E_{{\rm res},d} = 2$ MeV and $|M_{\rm GT}|^2 = 1$ in equation (27) gives a reasonable estimate of the electron capture rates (when the rates are appreciable and the temperature is too low for significant population of the GT^- back resonance) when $U_{\rm F} > 10$ MeV. These expressions can be used in place of our rate tables under these conditions. Using the simple approximations to the Fermi functions developed in Fuller et al. (1985) gives an analytic approximation to the high-density electron capture rates that is accurate to within the uncertainty in these rates. Electron capture rates for neutron-rich nuclei at high electron Fermi energies are essentially a function of only one parameter, the total GT^+ strength within a few MeV of the daughter state. Discrepancies between our calculated rates and more detailed calculations, e.g., Monte Carlo+RPA calculations (Langanke et al. 2001), largely reflect the difference between our adopted $|M_{\rm GT}|^2 = 1$ and the more detailed estimate of $M_{\rm GT}$.

Figure 14 also gives an estimate of the uncertainties in the electron capture rates. At $T_9 = 10$, $\rho Y_e = 3 \times 10^{10}$ g cm^{-3} ($U_f \approx 16$ MeV), an error of 2 MeV in the position of the centroid of the strength results in a change in the rate by a factor of $\sim$4 for the nuclei with the smallest rates, and a factor of $\sim$2 for the nuclei with the largest rates. At $T_9 = 10$, $\rho Y_e = 10^{11}$ g cm^{-3} ($U_f \approx 23$ MeV), the uncertainty in the placement of the centroid implies an error of at most a factor of 2 in the electron capture rate. On general grounds it is expected that not only the distribution of the configuration mixing strength, but also the magnitude of the total GT^+ strength, should vary from nucleus to nucleus for nearly GT^+-blocked nuclei. The uncertainty in the total strength is probably about a factor of 2 on average. This estimate is supported both by the charge exchange experiments discussed above as well as by the calculations of Sampaio et al. (2002; K. H. Langanke 2002, private communication) for $\sim$100 nuclei with $A > 65$, which show that the assignment of a constant strength of approximately unity is not too bad.

The systematics of the β-decay rates at high temperature and density are also simple. In Figure 15 we show the β-decay rates at $T_9 = 10$, $\rho Y_e = 10^{10}$ g cm^{-3} for all nuclei with $(N - Z/A) > 0.1$. These rates fall into three distinct bands corresponding to odd-odd nuclei, even-even nuclei, and even-odd/odd-even nuclei. This can be understood by noting that at $T_9 = 10$ the GT^+ resonance is thermally populated (under our assumption that the strength is centered at 2 MeV for these blocked nuclei). In this case the rate of decay is approximately $\lambda({\rm Q})Z_{\rm daughter}/Z_{\rm parent}$, where $\lambda({\rm Q})$ has a simple dependence on the Q-value. For even-even

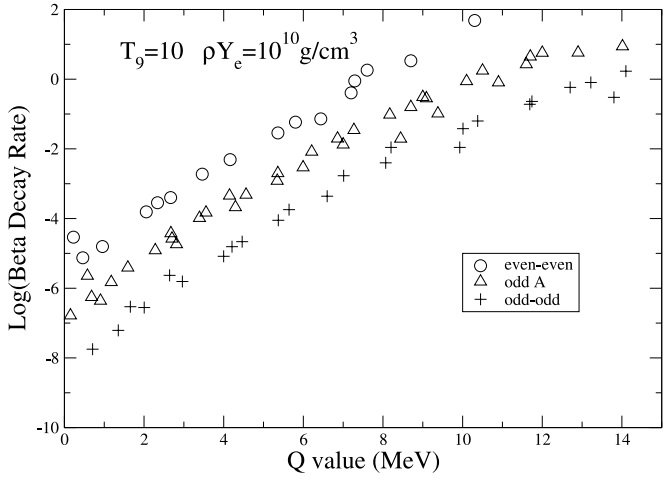

FIG. 15.—β-decay rates for neutron-rich nuclei in the mass range $65 < A \leq 80$ at $T_9 = 10$ and $\rho Y_e = 10^{10}$ g cm^{-3}. The systematics illustrated here are discussed in the text.

parents, $Z_{\rm daughter}/Z_{\rm parent}$ is typically approximately 20 at $T_9 = 10$, for odd-odd parents the ratio is about 1/20, and for odd-even/even-odd parents the ratio of partition functions is about unity. Note that the β-decay rates are more sensitive to the (unknown) details of the strength distribution than are the electron capture rates. At $T_9 = 10$, a 2 MeV error in the placement of the centroid of the resonance changes the β-decay rate by about an order of magnitude.

6.4. *Discussion and Conclusions*

We have provided estimates of weak interaction rates for nuclei in the mass range $A = 65$–80. These may be useful in simulations of X-ray bursts and presupernova stellar evolution. The rates have been calculated using available experimental information and simple estimates for the strength distributions and matrix elements for allowed and discrete-state transitions. The efficacy of our approach is confirmed through comparisons with detailed shell model based rates for nuclei in the mass range 60–65. However, the systematics of the strength distributions for nuclei in the mass range we are considering are arguably less well understood than the systematics of the strength distributions for nuclei in the mass range $A = 60$–65. As discussed above, uncertainties peculiar to the heavier nuclei we are studying can lead, in some cases, to sizeable uncertainties in the estimated rates.

The single most uncertain aspect of the rate calculations is the GT^+ resonance strength distribution. Our simple prescription gives good overall agreement with detailed shell model calculations of the GT^+ strength for nuclei with $A \leq 65$. However, our prescription is probably not reliable for nuclei at the end of the *fp* shell. Fortunately, nature to some extent does not seem to care about some of the hard to get details of the strength distribution for these nuclei. In the precollapse supernova this is because the nuclei present are nearly blocked to GT^+ transitions. Performing (n, p) exchange experiments on such nuclei shows that the strength is broad and low lying in the daughter. Because the electron Fermi energies are high in the dense presupernova Fe core, this implies that the electron capture rate is principally a function of the experimentally determined parent-daughter mass difference. However, our work does not

provide the detailed estimates of the magnitude of the configuration mixing strength that will ultimately also be needed for supernova simulations. The β-decay rates for the nuclei present in the late-time presupernova core are exponentially sensitive to the centroid energy of the GT^+ resonance and are less certain. In X-ray burst environments the opposite condition holds: the parent-daughter mass differences are typically large compared to the electron energies, so that the decay rate is dominated by the experimentally determined lifetime.

The proper treatment of the high-temperature electron capture and particularly β-decay rates is a challenging and important issue. Special care is needed in evaluating the partition functions for these rates, especially as we have pointed out here a potential problem with partition functions evaluated in Lanczos-based calculations. The β-decay rates for nuclei at high temperatures are determined, among other things, by the nuclear partition function. In turn, the equilibrium nuclear composition is determined by the competition between β-decay and electron capture. If the partition functions used to estimate the composition at a given Y_e do not match with the partition functions used to calculate the weak rates, the calculated equilibrium of the system will not be correct.

The authors acknowledge helpful correspondence with G. Martinez-Pinedo and K. Langanke regarding their calculations. We also thank Rob Hoffman for useful discussions regarding the *rp*-process. This work was partially supported by the DOE Program for Scientific Discovery through Advanced Computing (SciDAC) at UCSD and LLNL and by NSF grant PHY-00-0099499 at UCSD. A portion of this work was performed under the auspices of the US Department of Energy by University of California Lawrence Livermore Laboratory under contract W-7405-ENG-48.

REFERENCES

Aufderheide, M. B., Bloom, S. D., Mathews, G. J., & Resler, D. A. 1996, Phys. Rev. C, 53, 3139
Aufderheide, M. B., Brown, G. E., Kuo, T. T. S., Stout, D. B., & Vogel, P. 1990, ApJ, 362, 241
Aufderheide, M. B., Fushiki, I., Woosley, S. E., & Hartmann, D. H. 1994, ApJS, 91, 389
Bertsch, G. F., & Esbensen, H. 1987, Rep. Prog. Phys., 50, 607
Bethe, H. A., Brown, G. E., Applegate, J., & Lattimer, J. M. 1979, Nucl. Phys. A, 324, 487
Bloom, S. D., & Fuller, G. M. 1985, Nucl. Phys. A, 440, 511
Caurier, E., Langanke, K., Martinez-Pinedo, G., & Nowacki, F. 1999, Nucl. Phys. A, 653, 439
Cooperstein, J., & Wambach, J. 1984, Nucl. Phys. A, 420, 591
Fuller, G. M. 1982, ApJ, 252, 741
Fuller, G. M., Fowler, W. A., & Newman, M. J. 1980, ApJS, 42, 447 (FFNI)
———. 1982a, ApJ, 252, 715 (FFNII)
———. 1982b, ApJS, 48, 279
Fuller, G. M., Fowler, W. A., & Newman, M. J. 1985, ApJ, 293, 1
Gaarde, C., et al. 1981, Nucl. Phys. A, 369, 258
Helmer, R. L., et al. 1997, Phys. Rev. C, 55, 2802
Hillman, M., & Grover, J. R. 1969, Phys. Rev., 185, 1303
Langanke, K., Kolbe, E., & Dean, E. J. 2001, Phys. Rev. C, 63, 032801
Langanke, K., & Martinez-Pinedo, G. 2000, Nucl. Phys. A, 673, 481
Rauscher, T., & Thielemann, F. K. 2000, At. Data Nucl. Data Tables, 75, 1
Rowe, J. 1970, in Nuclear Collective Motion, Models and Theory (London: Methuen)
Sampaio, J. M., Langanke, K., Martinez-Pinedo, G., Kolbe, E., & Dean, D. J. 2002, preprint (nucl-th/0209057)
Sarriguren, P., de Guerra, E. M., & Escuderos, A. 2001, Nucl. Phys. A, 691, 631
Schatz, H., et al. 1998, Phys. Rep., 294, 167
———. 2001, Phys. Rev. Lett., 86, 3471
Vetterli, M. C., et al. 1992, Phys. Rev. C, 45, 997
Wallace, R. K., & Woosley, S. E. 1981, ApJS, 45, 389